JOURNAL OF Materials CHEMISTRY

Boronated carbons: structural characterization and low temperature physical properties of disordered solids

Bernard Ottaviani,[a] Alain Derré,*[a] Eusebiu Grivei,[b] Ould A. Mohamed Mahmoud,[c] Marie-Françoise Guimon,[c] Serge Flandrois[a] and Pierre Delhaès[a]

[a]*CRPP-CNRS, Avenue Albert Schweitzer, 33600 Pessac, France*
[b]*PCPM, Place Croix du Sud, 1 B-1348 Louvain-la-Neuve, Belgium*
[c]*LPCM, Avenue de l'Université, 64000 Pau, France*

B_xC_{1-x} compounds ($x \leqslant 0.25$) have been prepared by the thermal CVD technique. The aim of this paper is to better characterize some specific boron rich compositions that are not yet satisfactorily described. Both structural and physical properties have been investigated; including low temperature direct current resistivity, dynamic and static magnetic susceptibilities, specific heat and thermal conductivity. The final purpose is to correlate the structural disorder, both positional and substitutional, with particular electronic and vibrational properties deduced from low temperature experiments.

Because of several possible hybridizations and space organizations of carbon atoms, several polymorphic forms of pure carbon materials have been discovered. One possible extension of these materials is to introduce neighbouring atoms of the periodic classification in substitutional lattice positions, *i.e.* without changing the carbon network. Chemical preparations of mixed compositions consisting of carbon, boron and nitrogen atoms lead to modulating the electronic structure and the associated physical properties.[1] In the present work we are only interested in the most stable solid phase, *i.e.* the graphitic one (the hexagonal lattice is the thermodynamically stable structure).

The influence of boron doping on the layered carbon structure has been studied for forty years. The preparation of such binary compounds (B,C) can be divided into two categories.

(i) Chemical reactions at, or near, thermodynamic equilibrium which lead to low boron content materials. Lowell[2] has shown that the thermodynamic solubility of boron in the carbon lattice cannot exceed 2.35 atom%, and Marchand[3] summarized various techniques for doping graphitic carbons and graphites with boron (0.1–1 atom%).

Studying the diamagnetism behaviour *versus* temperature and based on the fact that the presence of boron atoms implies a decrease of the total π electron concentration, Soule[4] first demonstrated that boron atoms are mainly localized in substitutional sites (for boron content <1 atom%); Hall effect measurements allowed calculation of the charge carrier (holes) concentration associated with this atomic substitution.

Delhaès,[5] and Gasparoux *et al.*,[6] demonstrated the great sensitivity of electronic and magnetic properties to the boron content (boron <1 atom%) in pyrocarbons. Marchand and Dupart,[7] Zanchetta *et al.*[8] and Van der Hoeven *et al.*,[9] starting from the graphite band model[10] were able to explain the variation of magnetic, electronic and thermal properties for their samples (boron <0.23 atom%) by a lowering of the Fermi level inside the π valence band.

Jones and Thrower[11] and Hagio *et al.*[12] gave evidence for a simultaneous decrease of the crystallographic *c* parameter and a weak increase of the *a* parameter as the boron content increases (boron <5 atom%). These authors proposed both mechanical and chemical reasons to explain this behaviour, assuming that boron atoms are mainly substituted rather than intercalated in the graphitic lattice.

(ii) Chemical reactions which are not at equilibrium and give rise to non-crystalline solids with various boron contents; the resulting boron content is a function of the experimental process and of the initial phases.

Numerous techniques and precursors have been used[13,14] and most authors have generally extended their study to the ternary (B,C,N) system.[15–28] Chemical vapour deposition (CVD) has also been widely developed and we will now focus on these results.

Kouvetakis *et al.*,[29] starting from benzene and boron trichloride obtained for the first time the BC_3 global formula compound at 800 °C under reduced pressure. Thermal stability was good below 1200 °C, a temperature at which the B_4C type carbide begins to appear. Furthermore a room temperature resistivity value of 2.2×10^{-4} Ω cm was measured for BC_3, *i.e.* 10% lower than that for highly oriented pyrolytic graphite (HOPG). However, Shen[30] recently proposed a more realistic value of 2×10^{-3} Ω cm as well as a well ordered (periodic) structure for BC_3 which has been modelled by Lee and Kertesz,[31] Tomanek *et al.*,[32] Wentzcovitch *et al.*[33] and Mohamed Mahmoud and Loudet.[34] Two other ordered structures which could be imagined for BC_3 have been also modelled.

At higher temperatures, 800–1100 °C, and using acetylene instead of benzene, Saugnac *et al.*[35,36] and Derré *et al.*[37,38] also synthesized BC_3 and other compositions with lower boron contents. They studied the thermal stability for temperatures ranging from 1500 to 2500 °C and observed a decrease of both the d_{002} interlayer spacing and the full width at half maximum (FWHM). Nevertheless some phase separation occurs above 1750 °C leading to a B_4C+C biphasic mixture. ^{11}B NMR experiments could be interpreted in terms of the existence of B—B pairs in the carbon lattice, in agreement with one of the three proposed structures.[29] Electrical resistivity, magnetoresistance and Hall effect measurements showed an electrical behaviour with almost no temperature dependence; that charge carriers are mainly holes and finally, the weak localization effect, characteristic of a two-dimensional electronic system for BC_3.[38]

Jones and co-workers[39] also reported the formation of B_xC_{1-x} ($0.20 < x < 0.25$) as did Kouvetakis *et al.*, but for lower deposition temperatures, 500–800 °C. In this work, Raman microspectroscopy revealed that the BC_3 structural organization is very poor compared to a pyrocarbon or a weakly

doped pyrocarbon: nevertheless, the low deposition temperature of BC_3 (525 °C) could explain this observation.

The results of Kouvetakis and Jones concerning the CVD of B_xC_{1-x} films ($0<x<0.17$) were generalized by Way *et al.*[40] X-Ray diffraction (XRD) showed that the decrease of the *c* parameter observed for low boron materials continues for higher contents. Moreover, a sharp change from 3.41 to 3.34 Å ($d_{002}=3.354$ Å for pure crystalline graphite at room temperature) occurs between 12 and 15 atom%. These authors then proposed the existence of a BC_5 compound. Using synchrotron radiation and measuring the near-edge X-ray absorption at the carbon and boron 1s edges, they concluded that boron should be mainly substituted for carbon in these materials.

Finally, Hach *et al.*[41] have also studied BC_3 type compounds and XRD and Raman microspectroscopy experiments are in accord with the previous results.

Boron rich materials of B_xC_{1-x} type are not yet satisfactorily described and the goal of this work is to better characterize some specific boron rich compositions obtained by CVD in pregraphitic carbons. Both structural and physical properties have been investigated: in particular low temperature dynamic and static magnetic susceptibilities and thermal properties (specific heat and thermal conductivity) have been carefully studied. The final purpose is to correlate the structural disorder, both positional and substitutional, with the particular electronic and vibrational structures revealed by physical experiments carried out at liquid helium temperatures on these non-crystalline compounds.

Chemical deposition and boron content

B_xC_{1-x} materials were prepared by low pressure chemical vapor deposition (LPCVD). The total gas pressure in the alumina reactor was 30 mbar, the alumina substrate temperature was stabilized at 1100 °C, and the gases used for these manipulations were boron trichloride (5 to 10 $cm^3\ min^{-1}$), acetylene (11 $cm^3\ min^{-1}$) and hydrogen (477 $cm^3\ min^{-1}$). For boron trichloride, the flow was a function of the desired B/C ratio (Fig. 1). A more detailed description of the reactor we used is given elsewhere.[37]

All the compositions have been determined either by electron probe microanalysis (EPMA) or occasionally by Rutherford backscattering (RBS) or chemical analysis. Good agreement was found in the results of these different techniques (Table 1). This fact led us to consider the EPMA method as an accurate method for elemental analysis.

For bulk formulated BC_3, XPS showed that there is a variation of the composition which consists of a carbon excess at the outer surface of the sample. This inhomogeneity is observed for depths varying from 200 to 400 Å: this may be due to the LPCVD protocol. Indeed, at the end of the preparation, the BC_3 flow is first stopped and then that of the acetylene. During this short time, acetylene may lead to a pure carbon deposit responsible for the surface carbon excess. Below 400 Å, the composition appears to be stable with values indicated in Table 1 (30 min etching time). It should also be noted that similar inhomogeneity has been observed by the RBS technique. This surface composition is not important for the characterizations reported hereafter, the total thickness of the film being about 100 μm.

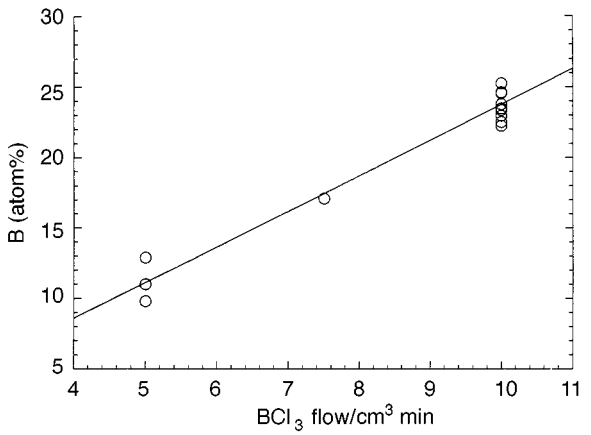

Fig. 1 Boron content *versus* BCl_3 flow

Table 1 Determination of the composition of B_xC_{1-x} samples by different analysis techniques

		composition (atom%)			XPS (etching time/min)		
sample	atom	elemental analysis	EPMA	RBS	0	15	30
BC_9(a)	B	9	10				
	C	90	90				
	O	1	0				
BC_9(b)	B		11				
	C		89				
	O		0				
$BC_{7.5}$	B	11	13				
	C	88	87				
	O	0	0				
BC_5	B		17				
	C		83				
	O		0				
BC_4	B	22	21	22			
	C	77	79	78			
	O	1	0	0			
$BC_{3.5}$(a)	B		23				
	C		77				
	O		0				
$BC_{3.5}$(b)	B		23				
	C		77				
	O		0				
$BC_{3.5}$(c)	B				0.0		23.1
	C				94.8		73.2
	O				4.1		1.7
$BC_{3.5}$(d)	B				1.4	8.0	23.2
	C				97.2	82.0	76.8
	O				1.4	0.0	0.0
BC_3(a)	B		25				
	C		75				
	O		0				
BC_3(b)	B		25				
	C		75				
	O		0				
$BC_{2.5}$	B				1.0	13.6	28.9
	C				97.0	86.3	70.6
	O				2.0	0.0	0.0

Structural properties

X-Ray diffraction and TEM study

A Siemens diffractometer with a Cu X-ray tube in a flat plate sample geometry and an Inel CPS 120 curved detector were used for diffraction experiments. The X-ray diffraction results of pure carbon (obtained at 1100 °C), BC_9 (10 atom%), BC_5 (17 atom%), BC_4 (20 atom%), and BC_3 (25 atom%) are summarized in Fig. 2. The FWHM of the (002) line for pyrocarbon is the most intense because of the deposition temperature which is quite low. The FWHM of BC_3 and BC_4 are as expected narrower than that of pure carbon owing to the presence of boron, but larger than that of BC_5 and BC_9. This indicates that the apparent crystallinity of BC_5 and BC_9 is better than that of BC_3 and BC_4. This is confirmed by the position of the (002) diffraction line which is greater for BC_3 and BC_4 than for BC_5 and BC_9. Fig. 2 clearly shows the existence of a minimum for both d_{002} and the FWHM lying around 10–15 atom% boron.

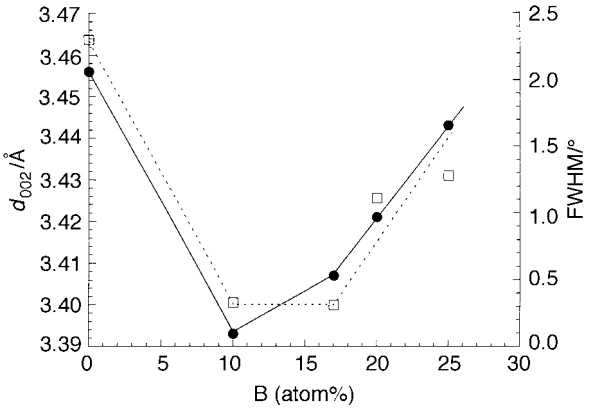

Fig. 2 d_{002} interplanar spacing (●) and full width at half maximum (FWHM; □) of the diffraction line as functions of boron content

BC_3 is deposited at 1100 °C, near the temperature limit for phase separation predicted by Kouvetakis,[29] but we do not detect any diffraction line corresponding to a boron carbide ($B_{13}C_2$ or B_4C). However, the absence of such lines is not sufficient to exclude the existence of a carbide phase. In fact, if boron carbide domains are small enough, or amorphous, it is possible that the XRD technique is not able to detect them.

In order to confirm these XRD results, we examined BC_3, BC_5 and BC_9 by transmission electron microscopy (TEM), using a JEOL 2000 FX instrument. Fig. 3 shows the direct lattice of these samples and the associated microdiffraction patterns. It is clear that BC_9 and BC_5 are more textured than BC_3. Indeed, in the latter, the microdiffraction pattern consists of continuous diffraction rings establishing a greater disorder than for the BC_9 sample. We verified that the integrity of these materials was not modified by the electron beam. Boron carbide was not detected, even using a high intensity beam.

Density measurements

Table 2 lists the interlayer spacing d_{002} measured by XRD and the corresponding experimental density (using a Micromeritics Accupyc 1330 helium pycnometer) and theoretical density, calculated with the relation:

$$d = \frac{Z\ (\text{atom\%}\ \text{B}M_{\text{B}} + \text{atom\%}\ \text{C}M_{\text{C}})}{2N_{\text{Av}}a^2 \sin(120) d_{002}} \qquad (1)$$

where Z is the number of atoms per unit cell of graphite, M_{B} the atomic mass of boron, M_{C} the atomic mass of carbon, N_{Av} the Avogadro number and a the in-plane lattice parameter of graphite. Relation (1) assumes that all the boron atoms are substituted for carbon atoms in the graphitic plane.

For BC_9 and BC_5, the experimental density is lower than the theoretical one, as expected. However, for BC_3, it is seen that the theoretical density is lower than the measured density which implies that the assumption of our model is not correct.

Thus, in order to take into account the increase of density observed in the BC_3 case, we must propose that some boron atoms are in interstitial positions.

XPS analysis

Table 3 and Fig. 4 show XPS results obtained for reference compounds (HOPG, elemental boron, a $B_{13}C_2$ film obtained by CVD and a commercial B_4C powder) and for different samples near the BC_3 stoichiometry. The analyses were performed using a Surface Science Instruments (SSI) spectrometer (model 301).

These results seem to indicate that BC_3 samples have specific B and C binding energies which are not the same as for B_4C or $B_{13}C_2$. Owing to the number of deconvoluted peaks for both the C 1s and B 1s edges, it is difficult to interpret categorically such spectra. Nevertheless we can propose the following possibility. The C 1s band is composed of three

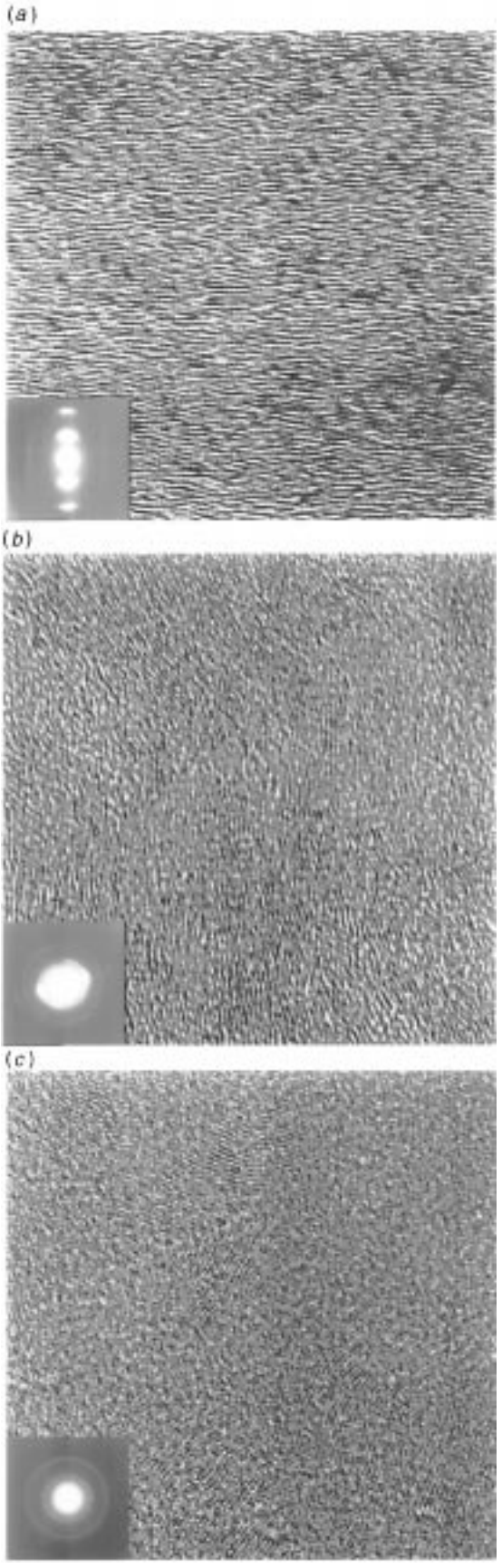

Fig. 3 TEM photographs of the direct lattice and associated microdiffraction pattern of BC_9 (*a*), BC_5 (*b*) and BC_3 (*c*)

Table 2 Interlayer spacing, experimental and theoretical densities of BC_9, BC_5, BC_4 and BC_3

sample	$d(002)$/Å	experimental density/g cm^{-3}	calculated density/g cm^{-3}
BC_9	3.393	2.147±0.028	2.217
BC_5	3.407	2.180±0.020	2.195
BC_4	3.421	2.190±0.035	2.177
BC_3	3.440	2.219±0.032	2.154

Table 3 XPS study of HOPG, elemental boron, a $B_{13}C_2$ film, B_4C powder and BC_3 samples

sample	edge	E_b/eV	relative intensity (%)	FWHM/eV
C(HOPG)	C 1s	284.6	100	
B(pure)	B 1s	186.8	67.2	1.5
		187.8	32.8	1.5
$B_{13}C_2$	B 1s	187.3	82.3	1.5
(film)		188.7	17.7	1.7
	C 1s	281.7	12.2	1.3
		284.6	65.1	1.0
		285.6	16.3	1.0
		286.7	6.4	1.1
B_4C	B 1s	187.6	76.5	1.6
(powder)		189.0	23.5	1.9
	C 1s	282.0	29.9	1.4
		284.6	56.7	1.7
		286.0	13.4	2.1
$BC_{3.5}$(c)[a]	B 1s	188.1	19.0	1.2
		189.1	49.9	1.3
		190.1	23.0	1.3
		191.4	8.1	1.5
	C 1s	283.2	25.2	1.5
		284.3	62.9	1.4
		285.6	11.9	1.4
$BC_{3.5}$(d)[a]	B 1s	188.1	25.9	1.2
		189.0	46.6	1.2
		190.1	18.8	1.2
		191.4	8.7	1.6
	C 1s	283.3	33.7	1.4
		284.2	51.0	1.2
		285.1	15.3	1.2
$BC_{2.5}$[a]	B 1s	188.1	13.5	1.3
		189.0	55.3	1.4
		189.9	21.9	1.4
		191.2	9.3	1.6
	C 1s	283.2	34.3	1.3
		284.2	46.3	1.1
		285.1	19.4	1.4

[a]After etching.

peaks at 283.2, 284.2, and 285.1 eV. The 284.2 eV peak looks like that from pure carbon and can be attributed to in-plane carbon atoms with no first neighbour boron. The 285.1 eV component corresponds to positively charged carbon and is usually observed for disordered carbons. The low energy signal at 283.2 eV denotes carbon atoms with negative charge as would be expected for in-plane carbon atoms having boron neighbour(s). For B 1s four contributions appear at 188.1, 189.1, 190.1 and 191.3 eV. The 188.1 eV peak is very similar to that for elemental boron and seems to indicate that clusters of boron atoms are present in BC_3 compounds. The three other components are attributed to positively charged boron atoms and should correspond to in-plane boron atoms with different numbers of carbon atoms as first neighbours (one to three). The large energy shift at 191.3 eV denotes boron atoms with a very strong electropositive surrounding, and possibly corresponds to boron atoms in interstitial sites, and under the influence of two adjacent carbon layers.

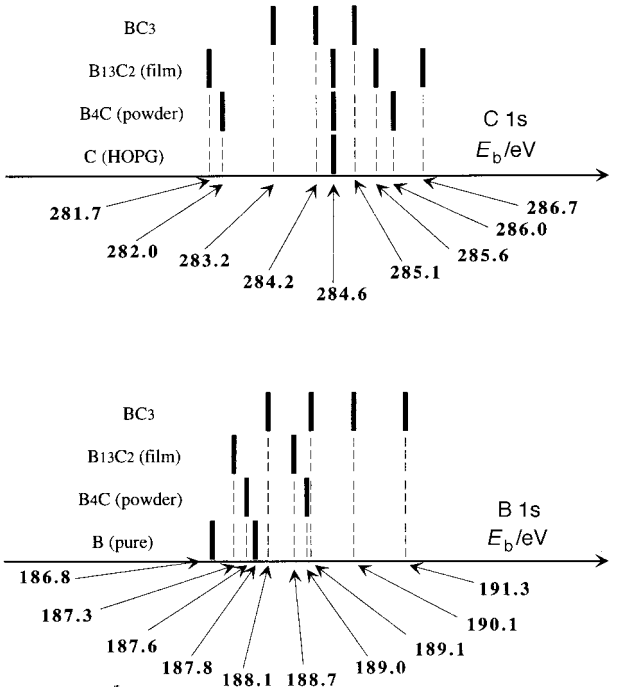

Fig. 4 Schematic representation of the XPS C 1s and B 1s binding energies for HOPG, elemental boron, $B_{13}C_2$ film, B_4C powder and BC_3 samples

Low temperature physical properties

Direct current electrical resistivity measurements

The standard four probe technique has been used to measure the electrical resistivity of BC_3, BC_5 and BC_9 samples from liquid helium to room temperature (Fig. 5).

Consistent with its better texture, BC_9 has the lowest resistivity and virtually no temperature dependence (relative variation 7%): this corresponds to a quasi-metallic (metallic alloy) behaviour. The resistivity increases with the increasing boron content, and finally, for BC_3 a smooth semiconducting regime is observed.

This behaviour is usually characteristic of semiconductor compounds, but for BC_3 the material retains a semimetallic character and presents weak localization behaviour.[42] The weak localization effect is due to the presence of defects in the lattice structure which reduces the mean free path of charge carriers. Filipozzi *et al.* showed the presence of such a phenomenon in BC_3 from magnetoresistance measurements.[43]

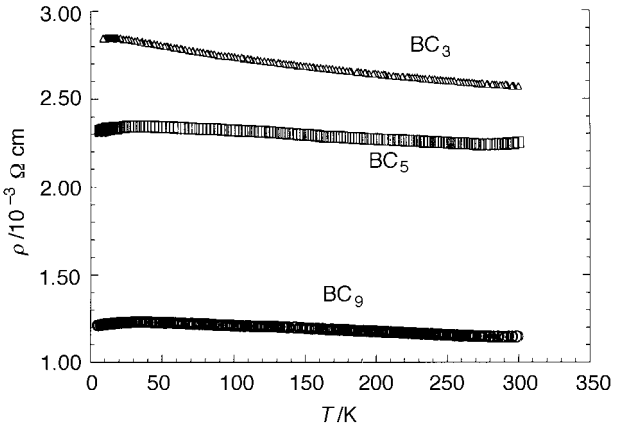

Fig. 5 Thermal variation of the dc electrical resistivity for BC_3, BC_5 and BC_9 samples

Magnetic properties and electronic structure

The electronic structure of B_xC_{1-x} compounds was probed using magnetization experiments using a superconducting quantum interference device (SQUID MS5 from Quantum Design) and EPR measurements (X-band spectrometer from Brücker equipped with an Oxford low temperature accessory). An important parameter to obtain, as far as the electronic properties are concerned, is the density of states at the Fermi level, $N(\varepsilon_F)$.

Static magnetism. The magnetic susceptibility χ_T is obtained from magnetization measurements at a given magnetic field ($H = 10$ kG). It can be expressed as the sum of different contributions:

$$\chi_T = \chi_c + \chi_L + \chi_{Pauli} + \chi_{Curie} \quad (2)$$

where χ_c is the diamagnetism due to the core electrons, χ_L the diamagnetism associated with the charge carriers (Landau diamagnetism), χ_{Pauli} is the charge carrier paramagnetism (temperature independent) and χ_{Curie} is the paramagnetism due to the trapped unpaired electrons (which usually varies as T^{-1}).

When the carbon sample presents a disorganized structure, χ_L becomes negligible. Then the χ_c term can be estimated using the Pascal systematics[44] and the χ_{Curie} term is deduced by plotting the values of χ_T *vs.* T^{-1}. In our case we obtained a straight line whose slope gave the Curie constant (C) and the χ_{Curie} term. The evaluation of χ_c (-5.19×10^{-7} and -5.38×10^{-7} emu g^{-1} for BC_9 and BC_3, respectively) and χ_{Curie} ($C = 3.40\times10^{-6}$ and 3.33×10^{-6} emu g^{-1} K^{-1} for BC_9 and BC_3, respectively) and the measurement of χ_T allow the calculation of χ_{Pauli} using eqn. (2). Fig. 6(*a*) and (*b*) show experimental results for BC_9 and BC_3, respectively.

The density of states at the Fermi level is then given by eqn. (3) which is strictly valid at 0 K (μ_B is the Bohr magneton).

$$\chi_{Pauli} = \mu_B{}^2 N(\varepsilon_F) \quad (3)$$

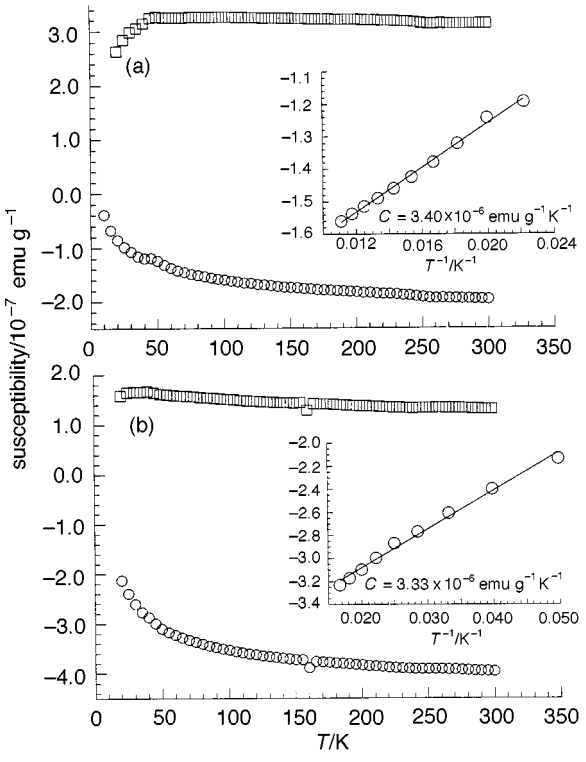

Fig. 6 Total (○) and Pauli (□) magnetic susceptibilities of BC_9 (a) and BC_3 (b), from 4 to 300 K. Total susceptibility *versus* reciprocal temperature is also illustrated in the insets.

Dynamic magnetism (EPR spectroscopy). In the case of EPR spectra for which one resonance line is obtained, we can directly obtain χ_{para} which is the sum of the χ_{Curie} and χ_{Pauli} terms (in the absence of any orbital contribution). A resonance line was observed only for the BC_3 compound (linewidth at room temperature $\Delta H = 4$ G with a g-factor of 2.0011). The EPR signal appears to be almost temperature independent down to 10 K; this implies that χ_{para} can be identified as the Pauli term (χ_{Pauli} *ca.* $3\pm0.3\times10^{-8}$ emu g^{-1}) and then the calculation of $N(\varepsilon_F)$ is simple *via* eqn. (3). We were not able to detect any EPR lines for the other samples which are assumed to be broadened owing to the existence of strong spin-relaxation mechanisms which are, as yet, not elucidated.

Thermal properties

Thermal conductivity. The temperature dependence of the thermal conductivity of BC_3 has been measured using a classical steady state thermal gradient.[45] This temperature dependence can be fitted by the elastic model developed by Kelly.[46] As pointed out by Nysten,[45] if the diffusion of phonons is limited by atomic defects and grain boundaries, *i.e.* with $\tau_{ph}{}^{-1} \propto \omega^3 v^{-2}$ where ω is the phonon pulsation and v their mean speed, a good numerical fit of the experimental data is obtained (Fig. 7). One of the adjustable parameters of this model is the shear modulus, C_{44}, one term of the elasticity tensor. This component is related to the force to apply to shift the graphitic planes with respect to each other in the planar direction. Thus, the higher the value of C_{44}, the higher is the coupling between the graphitic planes.

Specific heat (C_p) measurements. The low temperature specific heat has been measured using a relaxation time method which has been previously described.[47] It is well known that for lamellar compounds such as graphitic ones, there are two behaviour regimes for the lattice specific heat as a function of temperature.

At high temperature (up to 100 K), C_p follows a T^2 rule owing to the two-dimensional character of the lattice vibrations.

At low temperature (below *ca.* 10 K) C_p follows a polynomial rule expressed as follows:

$$C_p = \gamma T + \beta T^3 \quad (4)$$

The T^3 term which results from the vibrational coupling of graphitic planes is proportional to the usual three-dimensional Debye temperature (θ_D):

$$\theta_D = \left(\frac{12\pi^4 R}{5 M_{B_xC_{1-x}} \beta}\right)^{1/3} \quad (5)$$

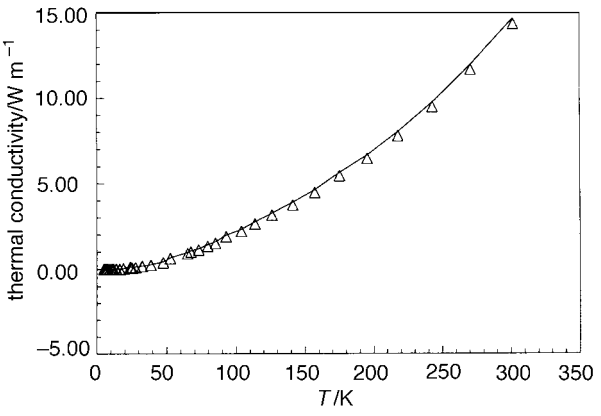

Fig. 7 Temperature dependence of the thermal conductivity of BC_3 and theoretical fit using Kelly's model[45]

where R is the macroscopic ideal gas constant and $M_{B_xC_{1-x}}$ the molecular mass of the BC_x compound.

The linear term is the consequence of the electronic contribution to the heat capacity in metals. This last term is usually coupled with $N(\varepsilon_F)$ by the relation:

$$N(\varepsilon_F)=\frac{3\gamma}{\pi^2 k_B{}^2} \quad (6)$$

where k_B is the Boltzmann constant

Fig. 8(*a*) and (*b*) show experimental measurements of the specific heat temperature dependences of BC_9 and BC_3, respectively, where the two expected terms are evident.

Analysis and Discussion

Here, we present comparisons between the experimental data and the theoretical model which will furnish new insight on the physical properties of these compounds.

Electronic structure and magnetic properties

The calculations presented hereafter are of two types: the first is based on the Slonsczewski–Weiss–McClure model (SWMcC) used for graphite and derivatives,[48] and the second is based on the *ab initio* Hartree–Fock linear combination of atomic orbital crystal orbital (STO-6G basis set) method (*ab initio* HF-LCAO-CO) using the Crystal 92 code.[34,49] This latter model is based on three-dimensional (ABAB stacking) calculations for the three hypothetical structures previously proposed for BC_3 [31] and takes into account the bielectronic repulsion inside the electron gas, which is not the case in the SWMcC model, which is based on the classical extended Hückel theory. Moreover, the *ab initio* HF-LCAO-CO theory takes into account the in-plane lattice geometrical deformations induced by the presence of boron whereas the SWMcC approach is a rigid band model.

Table 4 compares the values of $N(\varepsilon_F)$ obtained by the different theories and obtained from our experimental data.

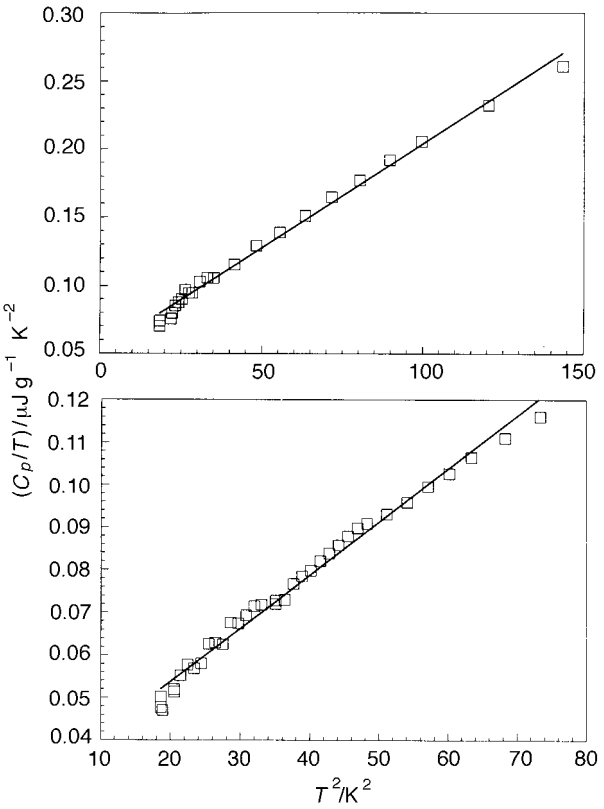

Fig. 8 C_p/T as a function of T^2 for BC_9 (*a*) and BC_3 (*b*)

Table 4 Comparative values of the density of states at the Fermi level calculated from experimental data and from theoretical models

	theoretical		experimental		
sample	*ab initio* HF-LCAO-CO	SWMcC model	SQUID magnet-ometer	ESR intensity line	specific heat linear term
graphite	4.6	4.6		4.64	5.85
BC_9		48.42	111.3	—[a]	277.8
BC_5		63.56	108.7	—[a]	
BC_3 1	15.6				
2	8.51	74.23	47.6	10.9	141.1
3	16.0				

[a]No signal.

The reference is hexagonal graphite where excellent agreement is observed. For boronated compounds, as expected, an increase of $N(\varepsilon_F)$ is observed but with rather large discrepancies between the different approaches.

For BC_9 and BC_5 the values given by the SWMcC model are lower than the values measured by SQUID measurements or EPR spectroscopy while the opposite is seen for BC_3. In this latter case this fact indicates that the $N(\varepsilon_F)$ values obtained from the SWMcC model are not consistent with the experimental data.

The $N(\varepsilon_F)$ values given by the *ab initio* HF-LCAO-CO method for BC_3 are nearer the experimental values than the SWMcC ones. This proves that the *ab initio* HF-LCAO-CO approach is superior to the SWMcC model even if lattice disorder is not considered.

We also note that the $N(\varepsilon_F)$ values given by specific heat measurements and calculated with relation (6) are always greater than those calculated from the SQUID and EPR measurements: this is possible because of the contribution of defects to the linear γ term[49,50] and establishes that there are many lattice defects in the structure of B_xC_{1-x} compounds. The existence of a linear term for low temperature specific heat, in excess of the straightforward electronic contribution, as in non-crystalline carbons,[49] is due to the presence of large structural disorder and therefore of localized phonons at weak energies. This is a signature of non-crystalline solids, together with the simultaneous presence of localized unpaired spins which obey the Curie law (Fig. 6) as already indicated for low temperature carbons.[50–51]

Vibrational structure and elastic properties

The C_{44} value obtained from the fit in the BC_3 case is 6.25 GPa, which is larger than that for graphite (4.4 GPa). Consequently, this higher value of C_{44} for BC_3 seems to prove that the coupling between the graphitic planes is stronger in BC_3 than in graphite. This observation is also confirmed by specific heat mesurements at low temperature.

It should be noted that the Debye temperature θ_D is also related to C_{44} and C_{33} (the compression modulus) by the following relationship:

$$\theta_D{}^3 = KC_{44}\sqrt{C_{33}} \quad (7)$$

where K is a proportionality factor.

This relationship arises from Komatsu's model[52] and is analogous to Kelly's model used for thermal conductivity[50] both of which are based on elasticity theory.

Table 5 lists values of θ_D for the different compounds. We can see that the value of θ_D for BC_3 is higher than that for graphite, while θ_D for BC_9 has an intermediate value. Using eqn. (7), we can assume that the higher value of θ_D for BC_3 compared to that of graphite is consistent with the observed increase of the shear modulus due to the presence of interstitial atoms.

Table 5 Comparative values of Debye temperature of Madagascar graphite,[49] turbostratic carbon,[49] BC_9 and BC_3 obtained from specific heat measurements

sample	Debye temperature/K
Madagascar graphite	450
turbostratic carbon	440
BC_9	480
BC_3	510

Conclusions

B_xC_{1-x} compounds have been prepared by the thermal CVD technique and characterized by several structural and physical methods. We distinguish two classes of materials. The boron poor ones seem to be single phases with a relatively well defined two-dimensional texture, while the boron rich ones are more disorganized but are still solid solutions of boron and carbon.

For lower boron concentrations, most of the boron atoms substitute for carbon atoms in the graphitic planes and thus give a well textured compound, while for higher boron concentrations, an increased amount of boron atoms is inserted between the graphitic planes.

All the techniques used and particularly XRD confirm the existence of these two families of boron doped compounds. This implies the existence of a critical boron concentration which separates the two zones. It is difficult to give an accurate value of the critical boron concentration at this time but the investigations we have made lead us to think that a value around 17 atom% B could be reasonable.

The low temperature physical properties show the presence of non-crystalline solids with a specific behaviour reminiscent of pregraphitic carbons. These properties are sensitive both to the lattice disorder in these lamellar solids and also to the deficiency of π electrons. These two effects are correlated, as shown by comparison with theoretical electronic and elastic models. They allow us to prepare new metastable compounds with specific properties which are of potential interest either for modified matrices in composites which are oxidation resistant at moderate to high temperature or as hosts for new intercalation compounds attractive for electrochemistry.

The authors wish to thank M. Chambon for precious help and collaboration in the TEM study, M. Loudet for theoretical calculations, R. Canet for electrical resistivity measurements, J. Amiell for EPR measurements, and finally L. Filipozzi, J. P. Issi, and B. Nysten for their assistance and their collaboration for specific heat and thermal conductivity measurements.

References

1 M. S. Dresselhaus, G. Dresselhaus and P. C. Eklund, *Science of Fullerenes and Carbon Nanotubes*, Academic Press, San Diego, CA, 1996.
2 C. E. Lowell, *J. Am. Ceram. Soc*., 1967, **50**, 142.
3 A. Marchand, *Chem. Phys. Carbon*, 1991, **7**, 175.
4 D. E. Soule, *5th Carbon Conf. Penn. State, Tome I*, 1961, p. 27.
5 P. Delhaès and A. Marchand, *Carbon*, 1965, **3**, 125.
6 H. Gasparoux, A. Pacault and E. Poquet, *Carbon*, 1965, **3**, 65.
7 A. Marchand and E. Dupart, *Carbon*, 1967, **5**, 453.
8 J. Zanchetta, P. Belougne and H. Gasparoux, *9th Conference on Carbon*, 1969, Boston, EP-11.
9 B. J. C. Van der Hœven, P. H. Keesom, J. W. McClure and G. Wagoner, *Phy. Rev*., 1996, **152**, 796.
10 B. T. Kelly, *Physics of Graphite*, Applied Science, London, 1981.
11 L. E. Jones and P. A. Thrower, *J. Chim. Phys*., 1987, **84**, 1431.
12 T. Hagio, M. Nakamizo and K. Kobayashi, *Carbon*, 1989, **27**, 259.
13 W. Cermignani, T. E. Paulson, C. Onneby and C. G. Pantano, *Carbon*, 1995, **33**, 367.
14 J. Kouvetakis, M. W. McElfresh and D. B. Beach, *Carbon*, 1994, **32**, 1129.
15 T. Y. Kosolapova, G. N. Makarenko, T. I. Serebryakova, E. V. Prilutskii, O. T. Khorpyakov and O. I. Chernysheva, *Pooshkovaya Metall*., 1971, **1**, 27.
16 T. V. Dubovik and T. V. Andreeva, *J. Less-Common Met*., 1986, **117**, 265.
17 L. Maya and L. A. Harris, *J. Am. Ceram. Soc*., 1990, **73**, 1912.
18 R. Riedel, J. Bill and G. Passing, *Adv. Mater*., 1991, **3**, 551.
19 J. Bill, M. Fiess and R. Riedel, *Eur. J. Solid State Inorg. Chem*., 1992, **29**, 195.
20 M. Kawaguchi, T. Kawashima and T. Nakajima, *Denki Kagaku*, 1993, **61**, 1403.
21 Y. G. Andreev and T. Lundström, *J. Alloys Compd*., 1994, **210**, 311.
22 A. R. Badzian, T. Niemyski, S. Appenheimer and E. Olkusnik, *Khim. Svyaz. Popurov. Polumetall*., 1972, 362.
23 A. W. Moore, S. L. Strong, G. L. Doll, M. S. Dresselhaus, I. L. Spain, C. W. Bowers, J. P. Issi and L. Piraux, *J. Appl. Phys*., 1989, **65**, 5109.
24 T. M. Bessmann, *J. Am. Ceram. Soc*., 1990, **73**, 2498.
25 M. Hubacek and T. Sato, *J. Solid State Chem*., 1995, **114**, 258.
26 M. Ishikawa, T. Nakamura, M. Morita, Y. Matsuda and M. Kawaguchi, *Denki Kagaku*, 1994, **62**, 897.
27 J. Kouvetakis, T. Sasaki, C. Shen, R. Hagiwara, M. Lerner, K. M. Krishnan and N. Bartlett, *Synth. Met*., 1989, **34**, 1.
28 M. Yamada, M. Nakaishi and K. Sugishima, *J. Electrochem. Soc*., 1990, **137**, 2242.
29 J. Kouvetakis, R. B. Kaner, M. L. Sattler and N. Bartlett, *J. Chem. Soc., Chem. Commun*., 1986, 1758.
30 C. Shen, Ph.D. Thesis, Berkeley, CA, 1992, ch. 3.
31 Y. S. Lee and M. Kertesz, *J. Chem. Soc., Chem. Commun*., 1988, 75.
32 D. Tomanek, R. M. Wentzcovitch, S. G. Louie and M. L. Cohen, *Phys. Rev. B*, 1988, **37**, 3134.
33 R. M. Wentzcovitch, M. L. Cohen and S. G. Louie, *Phys. Lett. A*, 1988, **131**, 457.
34 O. A. Mohamed-Mahmoud and M. Loudet, unpublished work.
35 F. Saugnac and A. Marchand, *C. R. Acad. Sci. Paris, II*, 1990, **310**, 187.
36 F. Saugnac, F. Teyssandier and A. Marchand, *J. Chim. Phys*., 1992, **89**, 1453.
37 A. Derré, L. Filipozzi and F. Peron, *J. Phys. IV*, 1993, **3**, 195.
38 L. Filipozzi, A. Derré, J. Conard, L. Piraux and A. Marchand, *Carbon*, 1995, **33**, 1747.
39 D. L. Fecko, L. E. Jones and P. A. Thrower, *Carbon*, 1993, **31**, 637.
40 B. M. Way, J. R. Dahn, T. Tiedje, K. Myrtle and M. Kasrai, *Phys. Rev. B*, 1992, **46**, 1697.
41 C. T. Hach, L. E. Jones, C. E. Crossland and P. A. Thrower, *Extended Abstracts of the 21st Biennal Conf. on Carbon*, Buffalo, NY, 1993, p. 641.
42 V. Bayot, PhD Thesis, Louvain-la-Neuve, Belgium, 1991.
43 L. Filipozzi, L. Piraux, A. Marchand, A. Derré, A. Adouard and M. Kynany-Alaoui, *J. Mater. Res*., 1997, **7**, 1711.
44 G. Foex, *Constantes Sélectionnées: Diamagnétisme et Paramagnétisme*, Masson, Paris, 1957.
45 B. Nysten, Ph.D. Thesis, Université Catholique de Louvain, Belgium, 1991.
46 B. T. Kelly, *Carbon*, 1968, **7**, 485.
47 E. Grivei, Ph.D. Thesis, Université Catholique de Louvain, Belgium, 1996.
48 M. S. Dresselhaus, G. Dresselhaus and J. E. Fisher, *Phys. Rev. B*, 1977, **15**, 3180.
49 C. Pisani, R. Dovesi and C. Roetti, *Lectures Notes in Chemistry 48: Hartree-Fock* ab initio *Treatment of Crystalline Systems*, Springer Verlag, Berlin, 1987.
50 P. Delhaès and Y. Hishiyama, *Carbon*, 1969, **8**, 31.
51 P. Delhaès and G. Blondet-Gonte, *Phys. Lett*., 1972, **40**, 242.
52 K. Komatsu, *J. Phys. Chem. Solids*, 1964, **25**, 707.

Paper 7/03625F; *Received* 27*th May*, 1997.